The Effect of Zn Content and Granulation Temperature on Zn Leaching in an Fe-Saturated $(Fe_X Zn_{(1-X)})_2 SiO_4$ System

Jakob Kero Andertun [1,*] **, Pasi Peltola** [2]**, Fredrik Engström** [1] **and Caisa Samuelsson** [1]

1   Division of Minerals and Metallurgical Engineering, Luleå University of Technology, 971 87 Luleå, Sweden; fredrik.i.engstrom@ltu.se (F.E.); caisa.samuelsson@ltu.se (C.S.)
2   Boliden Mineral AB, Boliden Rönnskär, 932 81 Skelleftehamn, Sweden; pasi.peltola@boliden.com
*   Correspondence: jakob.kero@ltu.se; Tel.: +46-920-493-511

Abstract: The zinc in the fayalite slag of copper smelters, in which Zn-containing raw materials are used, is mainly found to be in oxidic phases, such as glassy iron silicate. During the slag water granulation process, the molten slag is heated, whereby the granulated slag achieves varying granulation temperatures. Therefore, in this study, we aimed to characterize and assess the leaching behavior of a synthesized Fe-saturated $(Fe_X,Zn_{(1-X)})_2SiO_4$ system to understand the dependance of the zinc leaching behavior on the parameters of the ZnO content (1–10 wt.%) and granulation temperature (1300 or 1400 °C). It was found that the Zn leaching increased with the increasing Zn content and granulation temperature, using both batch and static pH leaching methods. Zn leaching was further increased at pH 5 using diluted nitric acid under oxidation conditions. Among the oxides in the samples—fayalite, spinel, and glass—glass was found to contribute to Zn leaching, owing to its weathering during pH-titration.

1. Introduction

Iron silicate slags, also called fayalite slags, are generated in copper smelters when silica is added as a fluxing agent in the copper concentrate smelting process. The silica reacts with the copper-containing raw materials in the smelting furnace. One of the purposes of slag is to separate contaminating elements from the copper matte that originate from the raw materials. Usually, some of the copper is lost to the slag. Copper recovery from the slag can be increased through extended slag processing, such as by the gravimetric settling of Cu-containing inclusions. Moreover, a few smelters deal with high Zn contents in the slag, originating from raw materials, or with the recycling of secondary Zn-containing materials. These smelters have specific Zn-cleaning processes, such as Zn fuming by carbothermal treatment. The ZnO solid solution (ss) in the slag is reduced to Zn(g) via pulverized carbon injection (PCI) and removed via slag treatment processes [1,2]. Extended gravimetric settling can be conducted in an electric heated furnace prior to granulation. During the settling process, the slag is continuously heated, resulting in a varied/increasing slag granulation temperature during the process step. The molten slag can, in an efficient way, become both solidified and granulated by water (or air) granulation to an amorphous granular material with <4 mm particle size, and there is no need for further crushing or grinding. The granulated fayalite slag is suitable as, for example, construction material, such as aggregates in roads and building grounds and abrasive media in blasting agents [3,4], which are also named in the Non-Ferrous Metal Industries Best Available Techniques (NFM-BAT) of the European Union.

The granulated fayalite slag contains mainly SiO_2, FeO_x, and minor amounts of CaO, Al_2O_3, and MgO, as well as trace elements such as Zn, Cu, Mn, and Ni [3]. The mineralogy of fayalite-type slag has been characterized in several studies [5–7]. The main and minor

elements, including Zn, were found in oxide phases such as fayalite, spinel, and glass in the slag system. In addition, Cu- and Ni-containing inclusions, such as sulfides and metal(loid)s, from the smelter raw materials were detected [8,9].

The correlation between the chemical composition of the copper smelter slag and leaching has been addressed in several studies [10–13]. The sulfide and metal(loid) granules contribute to the leaching of Cu, Ni, As, and Sb when present in a fayalite-type slag [14]. The leaching from inclusions such as copper sulfides and metals (matte and metalloids) can be minimized by decreasing the content of inclusions. Improved inclusion separation during slag treatment has been well studied [8,9,15,16].

Piatak et al. concluded that, of the various slag types, those from copper extraction (including smelter and converter slag) leach the highest concentration of Zn when using equivalent leaching methods [5]. In addition, the authors concluded in an earlier study that the slag mineralogy has an impact on the leaching of specific elements [14]. Alter (2005) discussed leaching differences depending on the copper-smelter-specific raw materials, slag chemistry, and metallurgical processing [10].

Shanmuganathan et al. 2008 showed that granulated copper smelter slag (fayalite type) with 0.13–0.17 wt.% Zn content leached 0.03–0.12 mg/L Zn [17], compared to 130 mg/L Zn for granulated Cu and Pb smelter slag (olivine type) with 6.0 wt.% Zn [18]. This comparison shows that the content and slag chemistry of smelter-specific slag trace elements can affect their potential use in external applications due to the risk of leaching and spreading elements, such as Zn, into the surrounding environment [19–21]. Both Lidelöw et al. 2017 and Ettler et al. 2014 noted that the leaching behavior of fayalite and olivine slags changes over time [22,23]. The former showed that the leaching of Zn initially increases, peaks after two years, and later decreases over time [22]. Ettler et al. indicated that the leaching of Zn from some olivine slags (Primary Pb slag) increases over time as the fayalite weathers [23]. The studied literature shows different conclusions regarding the zinc leaching behavior and dissolution of fayalite/olivine-type slags, depending on the slag chemistry and their raw materials.

Further, Kero Andertun et al. showed that the oxidic glass phase is responsible for Zn leaching in fayalite slag [14]. The Zn leaching behavior of the oxide phase in fayalite slag has not been addressed in the literature and is a subject for further investigation. Moreover, the effect of varying granulation temperature and increasing temperature during the granulation process in smelters and varying ZnO content in the oxidic fayalite-based system on leaching behavior has not yet been examined in the literature.

Therefore, in this study, we chose a synthetic fayalite–willemite (Fe_2SiO_4–Zn_2SiO_4) solid solution (ss) system and investigated its Zn leaching behavior. Our aims were to determine the influence of FeO/ZnO substitution and granulation temperature (1300 or 1400 °C) on the Zn leaching of water-granulated synthesized $(Fe_{(1-X)},Zn_X)_2SiO_4$ containing 1–10 wt.% ZnO. Our objectives were to characterize the granular materials regarding their composition and mineralogy and to characterize Zn leaching based on the use of two-stage batch leaching and static pH titration methods. The findings from this study provide an enhanced understanding of the properties of fayalite-type slags containing Zn raw materials regarding ZnO content, temperature control, and Zn leaching from the oxidic phases in the slag.

2. Materials and Methods

2.1. Materials

In this study, six samples of $(Fe_{(1-X)},Zn_X)_2SiO_4$ (ZFS) were synthesized in laboratory-scale trials, with three compositions containing 1, 5, or 10 wt.% ZnO. The chemicals Fe_2O_3 (Alfa Aesar, 98 wt.%, metal basis), Fe (Alfa Aesar, 99 wt.%, metal basis), SiO_2 (Alfa Aesar, 99 wt.%. metal basis), and ZnO (Acros Organics, 99.5 wt.%) were used for the synthesis. The main contaminating elements in the chemicals were Al, Ca, S, and Mg. The samples were homogenized by smelting at Fe saturation in Fe crucibles in a Tamman furnace at 1300 °C for 60 min at ambient pressure. Argon gas (Linde Gas AB, Stockholm, Sweden,

99.999%) maintained an inert atmosphere in the crucibles (3 L/min). After cooling to room temperature in the furnace, the 3 different ZFS compositions (2 times 3 samples) were remelted in a muffle furnace at 1300 (ZFS13) or 1400 °C (ZFS14) for 30 min in the iron crucibles and ambient air atmosphere before water granulation. The Zn vaporization in the furnaces was compensated for by adding 1.1 [24] and 1.6 times the required Zn amount for the 1300 and 1400 °C trials, respectively.

2.2. Granulation Method

The ZFS samples were granulated in a laboratory water granulation system. The crucibles containing the molten ZFS samples were tilted, and the molten material was poured out into a water tank (1.00 m × 0.46 m × 0.38 m) at the short side where water jets (total water flow of approximately 1.13 L per second from 9 nozzles with diameter Ø 2.9 mm and 16 nozzles with Ø 1.35 mm) splashed the molten material into granules. The granules were finally deposited in a water bath to cool down to room temperature. The granulated ZFS samples were collected and dried at 105 °C for 24 h and split into subsamples for characterization and leaching tests. This granulation system is described in detail in [25].

2.3. Characterization Methods

The chemical composition of the granulated samples was determined by the laboratory ALS Scandinavia AB, Sweden, using lithium metaborate digestion (ASTM D3682:2013 and ASTM D4503:2008), HNO3/HCl/HF digestion (SS EN 13656:2003), and inductively-coupled plasma sector field mass spectrometry (ICP–SFMS) (SS EN ISO 17294-2:2016 and EPA method 200.8:1994).

The mineralogy and microstructure of the samples were studied via powder X-ray diffraction (XRD) using a PANalytical Empyrean X-ray diffractometer and via scanning electron microscopy (SEM) on a Zeiss Gemini Merlin instrument equipped with an Oxford Instruments energy-dispersive spectroscopy (EDS) detector, respectively [14]. XRD was used to determine the crystalline phases, over a 2θ range of 10.0131–89.9891° with a step size of 0.0260° and to quantify the amorphous and crystalline matter in the samples by Rietveld refinement, over a 2θ range of 5.0089–151.3109° with a step size of 0.0130°. Both configurations used a copper Kα radiation source at a voltage of 45 mV and a current of 40 mA and a monochromator. $CaCO_3$ (10 wt.%; Alfa Aesar, 99.5 wt.%, metals basis) was used as an internal standard. The recorded XRD patterns were examined using Highscore Plus software and were matched with patterns from the Crystallography Open Database [26]. SEM–EDS measurements were conducted on carbon-coated and polished cross sections of bulk sample granules in epoxy molds and on carbon-coated granules before and after leaching tests (pH titration, 0.15–0.30 mm fraction). The SEM settings for the measurements were an acceleration voltage of 20 keV and an emission current of 1.0 nA. Both point analysis and mapping were used for qualitative and semi-quantitative measurements.

Micromeritics Flowsorb II 2300 was used to determine the specific surface areas, via BET (m^2/g), of the granulated sample fractions sized 0.15–0.30 and 0.30–0.60 mm.

Viscosity estimations (Poise) of the ZFS sample compositions at the granulation temperatures were performed via thermodynamic calculations using FactSage 8.1 software.

2.4. Leaching Methods

To compare the leachability of the different slag samples, leaching tests, as shown in Table 1, were conducted according to the two-stage batch leaching test at different liquid to solid ratios (L/S2 and 8), as specified in EN12457-3, and pH titration, performed as in an earlier paper by the authors [14]. The EN12457-3 test followed the standard protocol, except for the use of 25 g of solid with a size fraction of 0.3–0.6 mm and 50 mL (L/S2) or 200 mL (L/S8) of water (Milli-Q, Millipore). The leaching values (mg/kg) of the L/S2 and 8 were combined to obtain values for L/S10. For the pH titrations (pH 5), we used 10 g of 0.15–0.30 mm fractions with an initial water content of 100 mL. The samples were placed in

a filter cloth and dipped down into the leaching liquid in the reactor. Magnetic stirring was set to 960 rpm. Diluted HNO_3 acid (0.025 M) was added during the titration.

Table 1. Experimental conditions for leaching tests.

Leaching Method	Sample	Fraction (mm)	Sample (gram)	Liquid (mL)	L/S * (mL/gram)	pH	HNO₃ (M)
EN12457-3	Granules	0.30–0.60	25	50, 200	2, 8	-	-
pH-titration	Granules	0.15–0.30	8–10	80–100	10	5	0.025 M

* Liquid/solid.

Both methods were conducted at room temperature ($20 \pm 5\ °C$). The leachates obtained using both methods were filtered (0.45 μm) and acidified with concentrated HNO_3 (68 vol.%, VWR) at 1 vol.% of the leachate volume. The contents of the main elements Fe, Si, and Zn and contaminants Al, Ca, and Mg were analyzed by the laboratory ALS Scandinavia AB, Sweden, via inductively-coupled plasma with mass spectrometry (ICP–MS). Elemental concentrations in the leachates are presented as the average value (in milligrams per liter (mg/L), milligrams per kilogram (mg/kg), or milligrams per square meter (mg/m²)) of two samples with the associated standard deviations (St. dev).

3. Results and Discussion

3.1. Characterization of Samples

The chemical compositions of the granulated ZFS samples are presented in Table 2.

Table 2. Normalized chemical compositions determined by ICP–MS and material data of ZFS samples.

Component	Unit	ZFS13-01	ZFS13-05	ZFS13-10	ZFS14-01	ZFS14-05	ZFS14-10
Al_2O_3	wt.%	0.78	0.74	0.58	0.73	0.67	0.60
CaO	wt.%	0.12	0.11	0.08	0.05	0.05	0.02
SiO_2	wt.%	28.6	27.7	27.0	27.3	25.5	25.5
[1] FeO_X	wt.%	69.2	66.6	62.2	70.6	68.2	64.3
MgO	wt.%	0.05	0.03	0.02	0.01	0.02	0.01
ZnO	wt.%	0.88	4.45	9.84	1.03	5.36	9.26
S	wt.%	0.18	0.17	0.13	0.17	0.15	0.12
Other	wt.%	0.19	0.18	0.15	0.15	0.12	0.12
Sum.	wt.%	100.0	100.0	100.0	100.0	100.0	100.0
[2] LOI	wt.%	−6.83	−6.61	−6.07	−6.75	−6.41	−6.02
[3] d_{20}	μm	377	380	389	348	372	377
[4] BET 0.30–0.60 mm	m²/g	0.26	0.15	0.07	0.24	0.10	0.07
[4] BET 0.15–0.30 mm	m²/g	0.34	0.15	0.09	0.37	0.14	0.10
Specific density	g/cm³	4.03	4.04	4.05	4.06	4.08	4.12

[1] Based on total Fe content, Fe^{3+} was not determined; [2] loss on ignition at 1000 °C; [3] 20 wt.% of the samples was smaller than the value; [4] BET surface area measurement.

The compositions show that ZnO contents of 0.88–9.84 wt.% and 1.03–9.26 wt.% were observed for the ZFS13 and ZFS14 samples, respectively, in agreement with the predicted values. The negative loss on ignition (weight increase) at 1000 °C indicates oxidation due to the reaction of FeO_x with O_2 to form Fe_3O_4 and Fe_2O_3 [27].

In microstructure studies of the samples (Figure 1) via SEM, spherical granules and edgy granule fragments that contain cavities were observed in the sample cross sections.
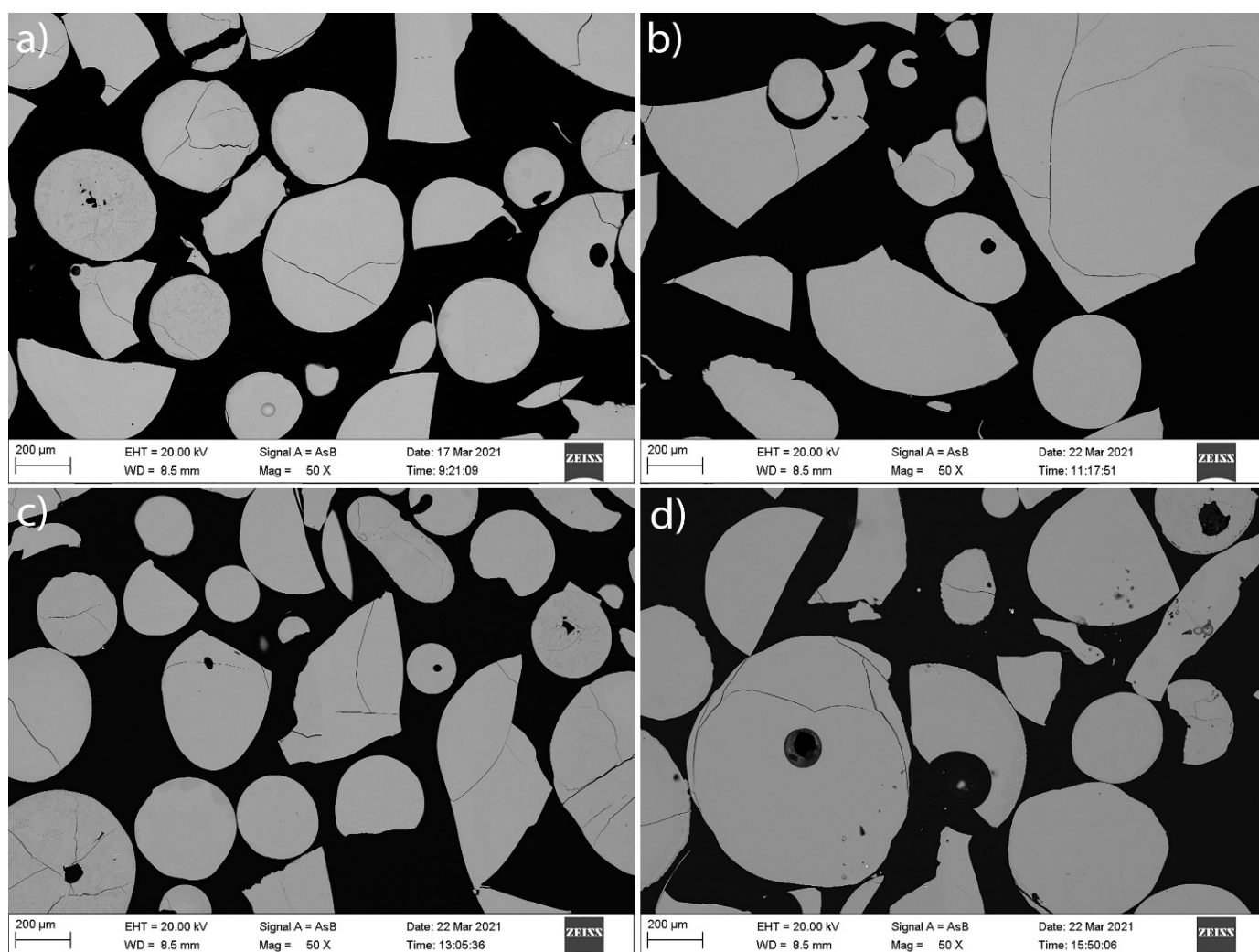
Figure 1. SEM–BSE images of granulated samples: (**a**) ZFS13-01; (**b**) ZFS13-10; (**c**) ZFS14-01; (**d**) ZFS14-10.

Based on XRD analysis (Figure 2a–c), it was determined that all samples contained crystals of mainly fayalite and a smaller amount of Fe–Zn spinel, which is in agreement with findings obtained by Wang et al. when studying fayalite–willemite-based materials with compositions similar to those in this study [28]. The humps found between 25 and 40° 2 theta indicate the presence of amorphous matter in all samples. ZnO/FeO substitution, resulting in increasing ZnO content, generated a peak shift owing to increasing ZnO content, a phenomenon that was earlier reported by Wang et al. [28]. The increase in the number of Zn atoms, with smaller radii than Fe atoms, in the $(Fe_{(1-X)},Zn_X)_2SiO_4$ samples resulted in decreased lattice constants, which caused the peak shift to the right [28].
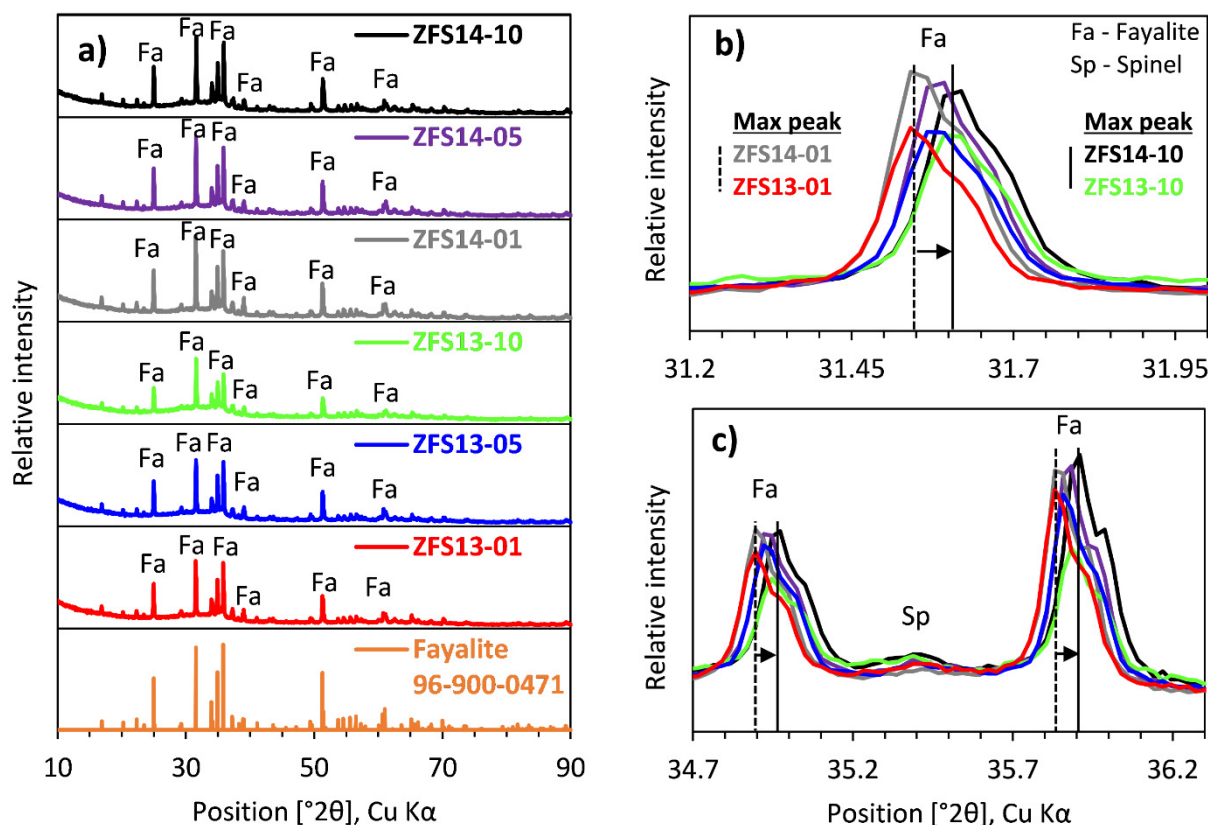
Figure 2. (**a**) X-ray patterns of ZFS samples containing 1, 5, and 10 wt.% ZnO for granulation temperatures of 1300 and 1400 °C; (**b**) main peak; (**c**) second and third peaks of Fa and main peak of Sp with peak shifts (black arrows). Fa, fayalite; Sp, spinel.

The Rietveld refinement (Table 3) results showed that the ZFS14 (granulated at 1400 °C) samples contained a higher amount of crystalline matter (18.6–20.8 wt.%) than the ZFS13 (granulated at 1300 °C) samples (11.3–16.8 wt.%). Lowered viscosity (Table 3) of the melts for ZFS14 compared to ZFS13 resulted in an increased crystallization rate, which generates a higher amount of crystalline matter in the ZFS14 samples. The crystallization rate was assumed to be constant, owing to constant particle size fractions and the water flow of granulation. On the other hand, an increasing ZnO content indicated a (partly) decreasing crystal content in the samples for ZFS13 and ZFS14. The calculated viscosities of the ZFS melts in Table 3 increased with the increasing ZnO content for both ZFS13 and ZFS14.

Table 3. Quantification of phases in the samples using Rietveld refinement and calculated viscosities at granulation temperatures using FactSage 8.1.

Sample	Fayalite, wt.%	Fe–Zn Spinel, wt.%	Amorphous wt.%	R_{Wp} *	Viscosity, Poise	Granulation T, °C
ZFS13-01	16.3	0.5	83.2	12.1	0.509	1300
ZFS13-05	14.8	0.2	85.0	13.1	0.561	1300
ZFS13-10	11.0	0.3	88.7	11.7	0.638	1300
ZFS14-01	20.1	0.7	79.2	13.6	0.348	1400
ZFS14-05	17.1	0.3	82.5	13.0	0.379	1400
ZFS14-10	17.8	0.8	81.5	12.0	0.425	1400

* Weighted profile R-factor.

The samples in Table 2 show varying surface areas depending on the ZnO content (0.26–0.07 m^2/g). For both the ZFS13 and ZFS14 samples, independent of granulation

temperature, the surface area decreased with the increasing ZnO content. The particle size distributions (d20, Table 2) became coarser grained with the increasing ZnO content. The increased viscosity (Table 3) is proof of the increasing particle size distribution, and this relationship has been previously presented in the literature [24].

The ZnO within the ZFS samples was, according to the EDS map (Figure 3a–d), distributed in both glass and crystalline microstructures. According to Wang et al., Zn is also likely distributed in fayalite and Fe–Zn spinel [28].
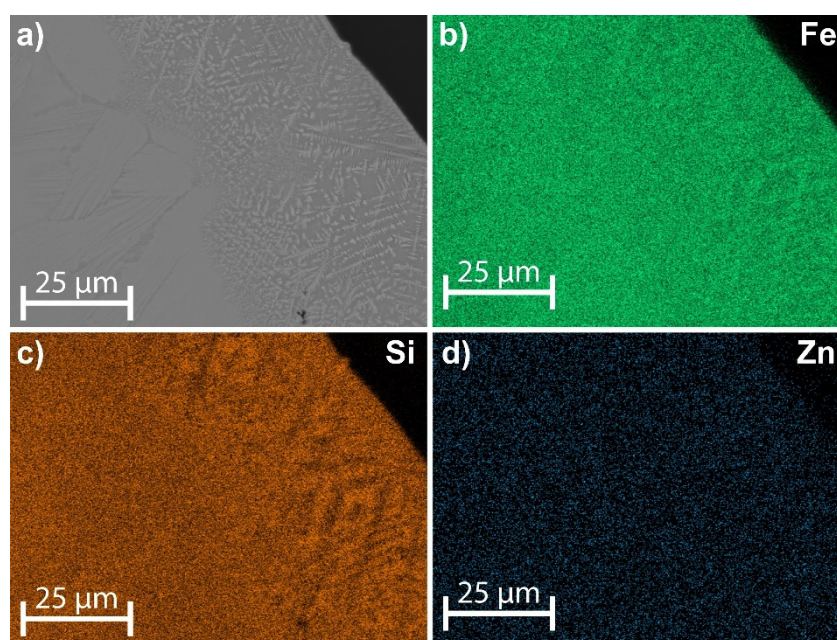

Figure 3. (**a**) SEM image including FeO_X crystals and matrix for ZFS13-01, and the distribution of (**b**) Fe, (**c**) Si, and (**d**) Zn.

3.2. Effect of ZnO Content on Zn Leaching

According to both the EN12457-3 and pH titration measurements, the ZnO content had an impact on the Zn leaching from the samples (Figure 4 and Table 4).
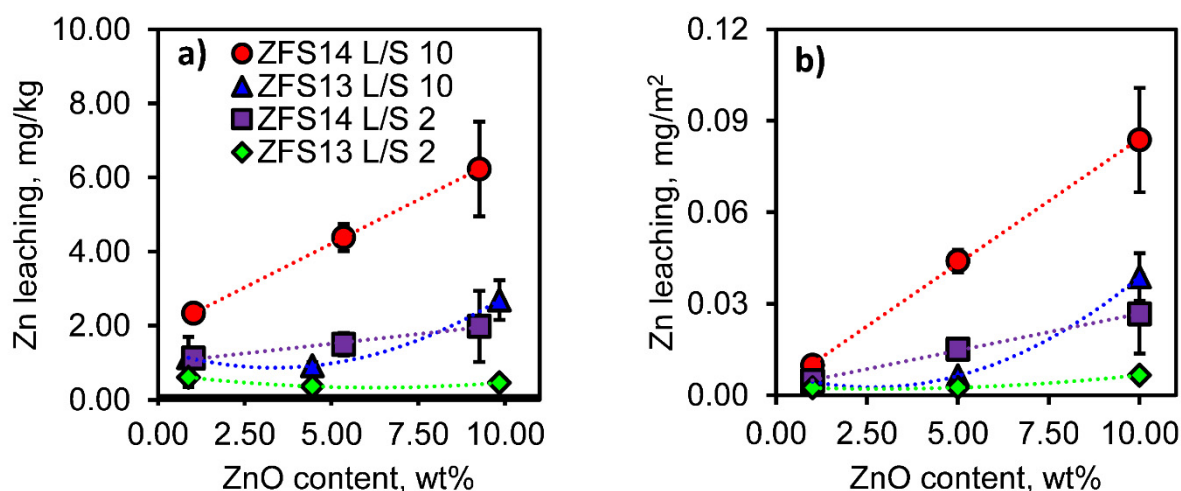

Figure 4. Zn leaching according to EN12457-3 versus normalized ZnO content in the ZFS samples: (**a**) mg/kg and (**b**) mg/m^2.

Table 4. Leaching data (mg/kg and mg/m^2) from leaching tests according to EN12457-3 and pH titration for the ZFS samples.

Sample	Unit	L/S2		L/S10		pH 5	
		mg/kg	mg/m^2	mg/kg	mg/m^2	mg/kg	mg/m^2
ZFS13-01	Average	0.61	0.0023	1.13	0.0044	17.5	0.0529
ZFS13-05	Average	0.36	0.0025	0.92	0.0063	33.0	0.228
ZFS13-10	Average	0.45	0.0065	2.69	0.0387	94.8	1.17
ZFS14-01	Average	1.12	0.0047	2.34	0.0097	13.0	0.0362
ZFS14-05	Average	1.50	0.0150	4.38	0.0440	74.5	0.554
ZFS14-10	Average	1.98	0.0266	6.23	0.0837	193	1.94
ZFS13-01	St. dev *	0.26	0.0010	0.57	0.0022	0.3	0.0035
ZFS13-05	St. dev	0.01	0.0001	0.10	0.0007	4.6	0.065
ZFS13-10	St. dev	0.06	0.0009	0.54	0.0078	3.1	0.23
ZFS14-01	St. dev	0.08	0.0003	0.12	0.0005	3.2	0.0022
ZFS14-05	St. dev	0.30	0.0030	0.37	0.0037	19.7	0.190
ZFS14-10	St. dev	0.96	0.0129	1.27	0.0171	15	0.04

* Standard deviation.

For both methods, Zn leaching increased with the increasing ZnO content in the samples, independent of granulation temperature. The EN12457-3 batch leaching test (Table S1) showed that pH values for L/S2 and L/S8 were in the ranges 6.4–7.3 and 6.5–7.0 for the ZFS13 and ZFS14 samples, respectively. The corresponding ranges for conductivity were 15.2–29.7 and 11.5–15.6 for L/S2 and 3.5–5.4 and 3.1–3.9 for L/S8 for the ZFS13 and ZFS14 samples, respectively. The conductivity of the leachates decreased with increasing ZnO content for both the ZFS13 and ZFS14 samples, indicating a lower amount of total dissolved solids (TDS), except for the L/S8 ZFS14 samples. This was explained by the reduced leaching of contaminating Ca (Table S2) as Zn leaching increased, resulting in an overall decrease in total leaching. The Zn leaching (Table 4) from EN12457-3 at L/S2 showed variation in the leaching values with increasing ZnO content for the ZFS13 and ZFS14 sample series in the ranges 0.36–0.61 mg/kg and 1.12–1.98 mg/kg, respectively. The leaching values calculated for L/S10 showed that Zn leaching increased for both the ZFS13 and ZFS14 series with the increasing ZnO content.

The pH titration measurements (Table 4) showed increased Zn leaching, with leaching values in the ranges 17.5–94.8 mg/kg and 13.0–193 mg/kg for ZFS13 and ZFS14 samples, respectively, as the ZnO content of samples increased.

The surface area of the samples were found to have an impact on Zn leaching. The BET measurements (Table 2) indicate that the surface area decreased with the increasing ZnO content for both ZFS13 and ZFS14 samples. However, Table 4 and Figure 4b show increasing Zn leaching per surface area (mg/m^2) at L/S10, and the leaching values with increasing ZnO content became even higher when comparing the 1–10 wt.% ZnO contents of the ZFS13 and ZFS14 samples. The increase in Zn leaching, despite the decreased surface area of the samples with increasing ZnO content, indicates that the leaching rates increased due to changes in sample composition.

3.3. Effect of Granulation Temperature on Zn Leaching

The granulation temperature was strongly correlated with the rate of Zn leaching (Table 4 and Figure 4a). For EN13457-3 batch leaching, increasing the granulation temperature from 1300 to 1400 °C resulted in increased Zn leaching independent of the ZnO content (1–10 wt.%) of the sample. Moreover, for static pH titration at pH 5, ZFS14 samples had higher Zn leaching values at 5–10 wt.% ZnO contents than the ZFS13 samples (Figure 5a,c).
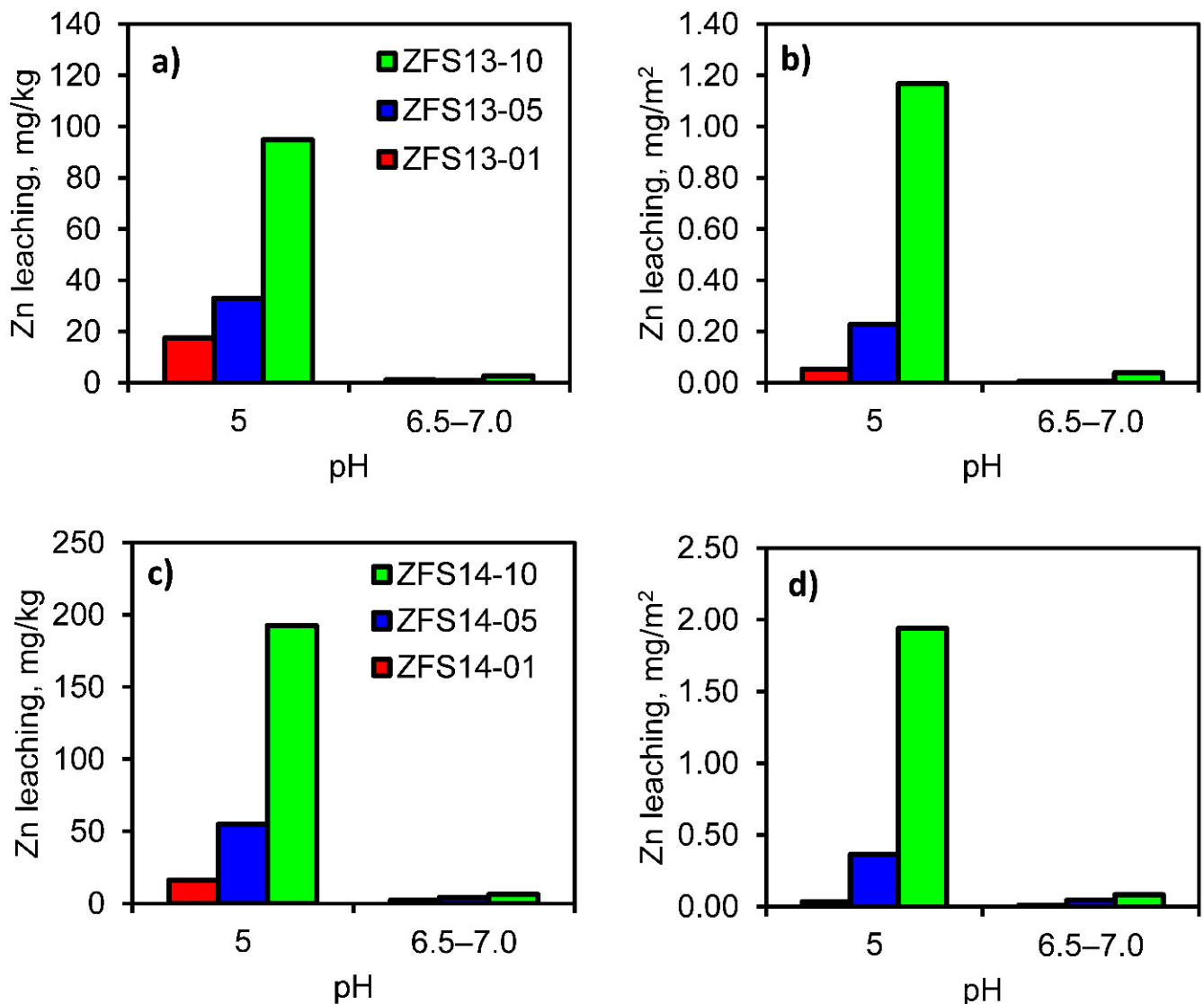
Figure 5. Zn leaching comparison versus pH for ZFS13, in (**a**) mg/kg and (**b**) mg/m^2, and for ZFS14, in (**c**) mg/kg and (**d**) mg/m^2.

The higher leaching values for ZFS14 samples indicate an impact of the thermal history for granulated (Fe$_{(1-X)}$,Zn$_X$)$_2$SiO$_4$, in a similar way as concluded for the granulated blast furnace slags (GBS) studied by Ehrenberg et al. 2020 [29]. The conclusion reached in their study was that the use of a higher granulation temperature for a granulated blast furnace slag results in increased reactivity regarding heat of hydration, owing to the higher enthalpy of the amorphous slag. Therefore, the higher enthalpy with higher granulation temperature might explain the greater Zn leaching from the ZFS14 samples compared to ZFS13 in this study. Further, the glass seems to contribute to Zn leaching, since SEM–EDS indicated there was weathering of the amorphous microstructure, while the crystalline microstructure at the rim remained more unaffected, as shown in Figure 6b,d. This interpretation is in alignment with the leaching behavior of the amorphous and crystalline slags reported by Potysz and Kierczak 2019 [30].
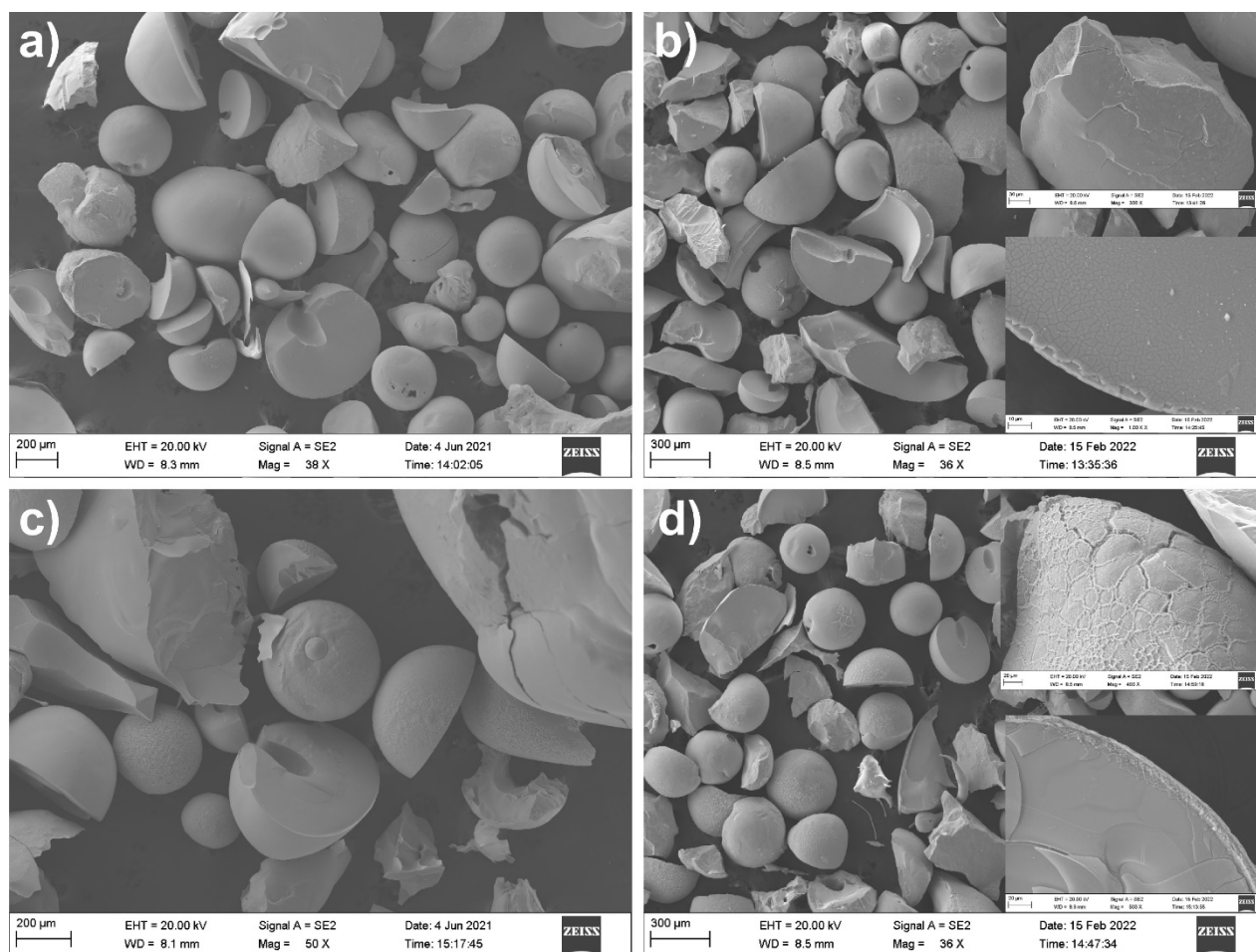
Figure 6. SEM images of sample surfaces for ZFS14-01 (**a**) before leaching and (**b**) after leaching at pH 5, and for ZFS14-10 (**c**) before leaching and (**d**) after leaching at pH 5.

3.4. Impact of pH and Sample Structure on Leaching

Figure 5a–d shows a comparison of the Zn leaching (L/S10) versus the pH for the EN13457-3 and pH titration samples, indicating that leaching increased as the pH decreased from neutral pH values (6.5–7.0) to 5. The increased Zn leaching with decreasing pH at oxidation conditions (using diluted nitric acid, 0.025M) was in accordance with the predominant phases in the Fe/Zn–O–H diagram, Figure S3. Moreover, the ratios of Zn/Fe leaching ([Zn]mg/kg/[Fe]mg/kg) at pH 5 increased (ZFS13: from 0.4 to 2.1, ZFS14: from 0.2 to 5.1) with the increasing Zn content for both ZFS13 and ZFS14 samples. Hence, the Zn became more reactive in comparison to Fe as the ZnO content increased.

The surface compositions of the samples were different from those of the bulk compositions according to SEM images of the sample microstructure, as seen in the cross sections (Figure 1a–d) and on the granule surfaces (Figure 6a–d). Figure 3a–d shows the microstructure of crystals and dendrites that formed at the granule surfaces during granulation.

The increase in Zn leaching was likely due to the formation of a more reactive Zn-containing phase/microstructure at sample surfaces, as seen in Figures 6d and 7a–d after static pH-titration. The Zn was predominantly distributed in the Zn-rich amorphous microstructure between the crystalline microstructures, as seen in Figure 7a–d. Further, this type of microstructure seemed to develop as the ZnO content increased. Figure 6d (in the top right-hand image) indicates that there was more leaching from the Zn-rich amorphous microstructure than from the overall crystalline microstructure, which might contribute substantially to the observed increase in Zn leaching with increasing ZnO content. At the same time, for both low and high ZnO contents in ZFS14-01 and ZFS14-10, the contributions

to leaching appeared to come from the amorphous microstructure, seen in Figure 6b,d, which is due to the microcrack formations on the granule surfaces, as has also been noted in the literature for steelmaking slag [31].
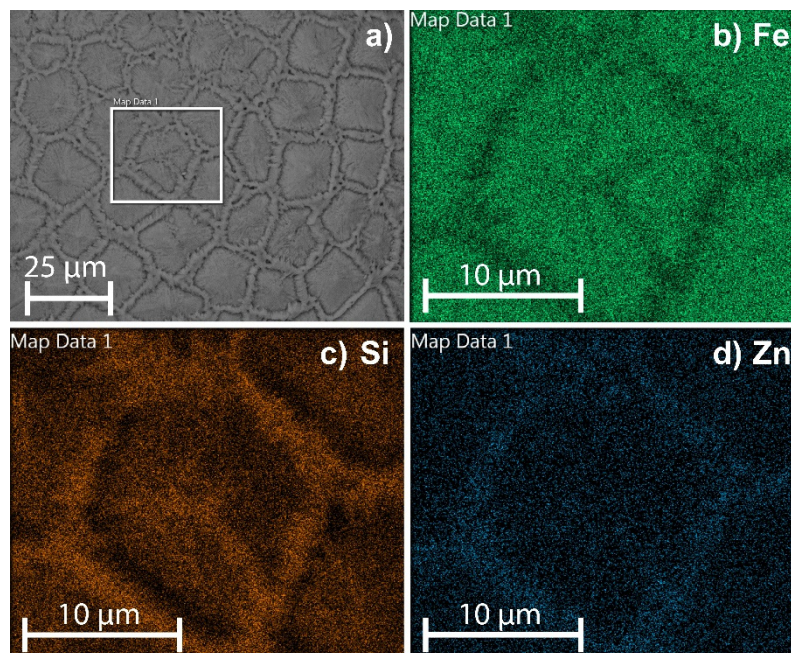

Figure 7. (**a**) SEM image and distribution of (**b**) Fe, (**c**) Si, and (**d**) Zn on sample surfaces of ZFS13-10 after static pH titration.

The Rietveld refinement results in Table 3 show a higher amount of crystalline matter in the ZFS14 compared to ZFS13 samples. However, the ZFS14 samples showed generally higher Zn leaching, which further indicates that Zn was predominantly distributed in the amorphous matrix at the granule surfaces.

3.5. Leaching Minimization

In this study, we investigated the leaching behavior of the synthesized $(Fe_{(1-X)},Zn_X)_2SiO_4$ system by varying the ZnO content and granulation temperature. The decrease in Zn leaching of the $(Fe_{(1-X)},Zn_X)_2SiO_4$ system was due to decreases in both the ZnO content and overheating (heating above the liquidus temperature) of the melt in the furnace to limit the granulation temperature. Zn leaching is mostly dependent on the granulation temperature and, according to Figure 4a,b, the leaching from ZFS13 increased between ZFS13-05 and ZFS13-10, while ZFS14 showed a continuous linear increase throughout the entire range of 1–10 wt.% ZnO. Thus, a lower granulation temperature limits the leaching from $(Fe_{(1-X)},Zn_X)_2SiO_4$ with higher ZnO contents up to 5 wt.%. Further, a lowered Zn content in the system limits the BET surface area of the sample granules, which prevents the leaching of other regulated compounds. These findings can be used to explain Zn leaching from different $ZnO–FeO_X–SiO_2$-containing materials.

4. Conclusions

From this research, we concluded the following:

- The granulated samples with the ZnO addition contain a mixture of crystalline fayalite, Fe/Zn spinel, and an amorphous microstructure, with ZnO dissolved in both the crystalline and amorphous phases.
- An increase in ZnO in the sample was correlated with decreased surface area of the sample granules, increased viscosity at the granulation temperature, and increased amorphous content.

- Zn leaching increased with increases in both granulation temperature and ZnO content for both the two-stage batch leaching and static pH titration in dilute nitric acid. The decreased surface area indicated increased Zn leaching reactivity.
- A higher granulation temperature resulted in higher Zn leaching values due to increased Zn reactivity.
- To avoid Zn leaching from materials with similar chemistry to those examined in this study, such as fayalite-type slags, the Zn content should be minimized and overheating of the melt prior to water granulation should be limited.

Supplementary Materials: The following supporting information can be downloaded at: https://www.mdpi.com/article/10.3390/min12060767/s1, Figure S1: Pourbaix diagrams plotted using FactSage 8.3, m = 0.001 mol/kg, T = 20 °C: (a) Fe–O–H and (b) Zn–O–H.; Table S1: Leaching data for EN12457-3 with pH, conductivity, and redox with standard deviations, n = 2.; Table S2: Leaching data for EN12457-3 with average leaching values and standard deviations, n = 2.; Table S3: Leaching data for static pH titrations at pH 5 with average values and standard deviations, n = 2.

Institutional Review Board Statement: Not applicable.

Data Availability Statement: The data presented in this study are available in the article or supplementary material.

Conflicts of Interest: The authors declare no conflict of interest.

References

1. Lotfian, S.; Vikström, T.; Lennartsson, A.; Björkman, B.; Ahmed, H.; Samuelsson, C. Plastic-containing materials as alternative reductants for base metal production. *Can. Metall. Q.* **2019**, *58*, 164–176. [CrossRef]
2. Maweja, K.; Mukongo, T.; Mutombo, I. Cleaning of a copper matte smelting slag from a water-jacket furnace by direct reduction of heavy metals. *J. Hazard. Mater.* **2009**, *164*, 856–862. [CrossRef]
3. Gorai, B.; Jana, R.K. Premchand Characteristics and utilisation of copper slag—A review. *Resour. Conserv. Recycl.* **2003**, *39*, 299–313. [CrossRef]
4. Dash, M.K.; Patro, S.K.; Rath, A.K. Sustainable use of industrial-waste as partial replacement of fine aggregate for preparation of concrete—A review. *Int. J. Sustain. Built Environ.* **2016**, *5*, 484–516. [CrossRef]
5. Piatak, N.M.; Parsons, M.B.; Seal, R.R. Characteristics and environmental aspects of slag: A review. *Appl. Geochem.* **2015**, *57*, 236–266. [CrossRef]
6. Potysz, A.; Kierczak, J.; Fuchs, Y.; Grybos, M.; Guibaud, G.; Lens, P.N.L.; van Hullebusch, E.D. Characterization and pH-dependent leaching behaviour of historical and modern copper slags. *J. Geochem. Explor.* **2016**, *160*, 1–15. [CrossRef]
7. Das, B.; Mishra, B.K.; Angadi, S.; Pradhan, S.K.; Prakash, S.; Mohanty, J. Characterization and recovery of copper values from discarded slag. *Waste Manag. Res. J. A Sustain. Circ. Econ.* **2010**, *28*, 561–567. [CrossRef]
8. Bellemans, I.; de Wilde, E.; Moelans, N.; Verbeken, K. Metal losses in pyrometallurgical operations—A review. *Adv. Colloid Interface Sci.* **2018**, *255*, 47–63. [CrossRef] [PubMed]
9. Schlesinger, M.E.; King, M.J.; Sole, K.C.; Davenport, W.G. Copper Loss in Slag. In *Extractive Metallurgy of Copper*, 5th ed.; Elsevier: Oxford, UK, 2011; pp. 191–203.
10. Alter, H. The composition and environmental hazard of copper slags in the context of the Basel Convention. *Resour. Conserv. Recycl.* **2005**, *43*, 353–360. [CrossRef]
11. Jarošíková, A.; Ettler, V.; Mihaljevič, M.; Kříbek, B.; Mapani, B. The pH-dependent leaching behavior of slags from various stages of a copper smelting process: Environmental implications. *J. Environ. Manag.* **2017**, *187*, 178–186. [CrossRef]

12. Kierczak, J.; Potysz, A.; Pietranik, A.; Tyszka, R.; Modelska, M.; Néel, C.; Ettler, V.; Mihaljevič, M. Environmental impact of the historical Cu smelting in the Rudawy Janowickie Mountains (south-western Poland). *J. Geochem. Explor.* **2013**, *124*, 183–194. [CrossRef]

13. Piatak, N.M. Environmental Characteristics and Utilization Potential of Metallurgical Slag. In *Environmental Geochemistry: Site Characterization, Data Analysis and Case Histories*, 2nd ed.; Elsevier: Amsterdam, The Netherlands, 2018; pp. 487–519. ISBN 9780444637635.

14. Kero Andertun, J.; Samuelsson, C.; Peltola, P.; Engström, F. Characterisation and leaching behaviour of granulated iron silicate slag constituents. *Can. Metall. Q.* **2022**, *61*, 14–23. [CrossRef]

15. Wang, X.; Geysen, D.; Tinoco, S.V.P.; D'Hoker, N.; van Gerven, T.; Blanpain, B. Characterisation of copper slag in view of metal recovery. *Miner. Processing Extr. Metall.* **2015**, *124*, 83–87. [CrossRef]

16. Jalkanen, H.; Vehviläinen, J.; Poijärvi, J. Copper in solidified copper smelter slags. *Scand. J. Metall.* **2003**, *32*, 65–70. [CrossRef]

17. Shanmuganathan, P.; Lakshmipathiraj, P.; Srikanth, S.; Nachiappan, A.L.; Sumathy, A. Toxicity characterization and long-term stability studies on copper slag from the ISASMELT process. *Resour. Conserv. Recycl.* **2008**, *52*, 601–611. [CrossRef]

18. Ettler, V.; Johan, Z.; Kříbek, B.; Šebek, O.; Mihaljevič, M. Mineralogy and environmental stability of slags from the Tsumeb smelter, Namibia. *Appl. Geochem.* **2009**, *24*, 1–15. [CrossRef]

19. Król, A.; Mizerna, K.; Bożym, M. An assessment of pH-dependent release and mobility of heavy metals from metallurgical slag. *J. Hazard. Mater.* **2020**, *384*, 121502. [CrossRef] [PubMed]

20. Schmukat, A.; Duester, L.; Goryunova, E.; Ecker, D.; Heininger, P.; Ternes, T.A. Influence of environmental parameters and of their interactions on the release of metal(loid)s from a construction material in hydraulic engineering. *J. Hazard. Mater.* **2016**, *304*, 58–65. [CrossRef]

21. Piatak, N.M.; Seal, R.R.; Hammarstrom, J.M. Mineralogical and geochemical controls on the release of trace elements from slag produced by base- and precious-metal smelting at abandoned mine sites. *Appl. Geochem.* **2004**, *19*, 1039–1064. [CrossRef]

22. Lidelöw, S.; Mácsik, J.; Carabante, I.; Kumpiene, J. Leaching behaviour of copper slag, construction and demolition waste and crushed rock used in a full-scale road construction. *J. Environ. Manag.* **2017**, *204*, 695–703. [CrossRef]

23. Ettler, V.; Johan, Z. 12years of leaching of contaminants from Pb smelter slags: Geochemical/mineralogical controls and slag recycling potential. *Appl. Geochem.* **2014**, *40*, 97–103. [CrossRef]

24. Lü, J.; Jin, Z.; Yang, H.; Tong, L.; Chen, G.; Xiao, F. Effect of the CaO/SiO$_2$ mass ratio and FeO content on the viscosity of CaO–SiO$_2$–"FeO"–12wt%ZnO–3wt%Al$_2$O$_3$ slags. *Int. J. Miner. Metall. Mater.* **2017**, *24*, 756–767. [CrossRef]

25. Feng, Y.; Yang, Q.; Chen, Q.; Kero, J.; Andersson, A.; Ahmed, H.; Engström, F.; Samuelsson, C. Characterization and evaluation of the pozzolanic activity of granulated copper slag modified with CaO. *J. Clean. Prod.* **2019**, *232*, 1112–1120. [CrossRef]

26. Gražulis, S.; Daškevič, A.; Merkys, A.; Chateigner, D.; Lutterotti, L.; Quirós, M.; Serebryanaya, N.R.; Moeck, P.; Downs, R.T.; le Bail, A. Crystallography Open Database (COD): An open-access collection of crystal structures and platform for world-wide collaboration. *Nucleic Acids Res.* **2012**, *40*, D420–D427. [CrossRef] [PubMed]

27. Li, Q.; Yang, F.; Wang, Z.; Liu, S. Study on Mechanism of Oxidation Modification of Copper Slag. *Trans. Indian Inst. Met.* **2019**, *72*, 3223–3231. [CrossRef]

28. Wang, Z.; Zhao, Z.; Zhang, L.; Liu, F.; Peng, B.; Chai, L.; Liu, D.; Liu, D.; Wang, T.; Liu, H.; et al. Formation mechanism of zinc-doped fayalite (Fe$_{2-x}$Zn$_x$SiO$_4$) slag during copper smelting. *J. Hazard. Mater.* **2019**, *364*, 488–498. [CrossRef]

29. Ehrenberg, A.; Romero Sarcos, N.; Hart, D.; Bornhöft, H.; Deubener, J. Influence of the Thermal History of Granulated Blast Furnace Slags on Their Latent Hydraulic Reactivity in Cementitious Systems. *J. Sustain. Metall.* **2020**, *6*, 207–215. [CrossRef]

30. Potysz, A.; Kierczak, J. Prospective (Bio) leaching of Historical Copper Slags as an Alternative to Their Disposal. *Minerals* **2019**, *9*, 542. [CrossRef]

31. Koizumi, S.; Xu, G.; Sukenaga, S.; Kanehashi, K.; Takahashi, T.; Ueda, S.; Kitamura, S.-Y. Influence of Glass Structure on the Dissolution Behavior of Fe from Glassy Slag of CaO-SiO$_2$-FeOx System. *J. Sustain. Metall.* **2021**, *7*, 583–596. [CrossRef]